Epitaxial orientation of MnAs layers grown on GaAs surfaces by means of solid-state crystallization

Y. Takagaki, C. Herrmann, B. Jenichen, and O. Brandt
Paul-Drude-Institut für Festkörperelektronik, Hausvogteiplatz 5-7, 10117 Berlin, Germany
(Received 13 June 2008; published 25 August 2008)

MnAs layers are grown on GaAs substrates employing solid-state epitaxy following deposition in a molecular-beam epitaxy system. The surface morphology varies markedly with the orientation of the substrates. This dependence is strictly dictated by the lattice mismatch in the direction of the *c* axis of MnAs. That the lattice mismatch is by far more important than interfacial atomic bonding in solid-state epitaxy provides an explanation that the minimization of the strain energy favors the *M*-plane orientation to the *C*-plane orientation on GaAs(111) despite the incompatible symmetries of the participating lattices.

DOI: 10.1103/PhysRevB.78.064115 PACS number(s): 68.35.−p, 64.70.K−

I. INTRODUCTION

In heteroepitaxy, the compatibility of the symmetry of the respective lattice planes generally plays the most critical role in determining the epitaxial orientation relationship. A consequential guiding principle in the growth of a hexagonal crystal is that the *c* axis is aligned normal to the surface on threefold- or sixfold-symmetric substrates, whereas it lies in the surface plane on twofold- or fourfold-symmetric substrates.[1] For MnAs layers on GaAs(111)B, however, a growth procedure has been discovered recently that gives rise to a symmetry-mismatched $(1\bar{1}00)$ orientation.[2]

MnAs is a ferromagnetic material having the NiAs-type hexagonal crystal structure. Because of the high Curie temperature (about 40 °C) and the possibility of epitaxy on GaAs and Si, the material is attractive for applications in spintronics.[3,4] A spin injection from MnAs into GaAs, for instance, has been demonstrated in Refs. 5 and 6. The magnetic hard axis of bulk MnAs is along the *c* axis, and so the controllability of the *c*-axis orientation is advantageous for applications. The in-plane magnetization is practically isotropic in *C*-plane MnAs layers, whereas *M*-plane layers exhibit a strong uniaxial magnetocrystalline anisotropy that can even overcome the shape anisotropy.[7] In addition, the lattice constant in the *a*-axis direction changes abruptly by a few percentage at the phase transition between the ferromagnetic α phase and the nonmagnetic β phase. The strain in epitaxial layers at the low-temperature phase, as a consequence, depends enormously on the angle of the *c* axis with respect to the substrate. The temperature range for the coexistence of α- and β-MnAs (Ref. 8) and the Curie temperature[9] are significantly influenced by the strain.

The unusual epitaxial orientation relationship MnAs$(1\bar{1}00)$/GaAs(111) is realized by solid-state epitaxy (SSE) following the deposition of a thin amorphous MnAs layer in a molecular-beam epitaxy (MBE) chamber.[2] Amorphous deposition is achieved by reducing the substrate temperature to a value lower than that used for conventional MBE. Solid-state crystallization is induced by decreasing the background As pressure and increasing the substrate temperature. While the thickness of the amorphous layer being larger than the limit for coherent growth was speculated to be crucial, the mechanism that leads to the symmetry-mismatched *M*-plane surface orientation has not yet been identified.

In this work, we apply the SSE-based growth to various surface orientations of GaAs substrates, see Fig. 1. The results range from a monocrystalline alignment for (110)-oriented substrates to a mixture of different surface orientations and in-plane tilts for (001)- and (113)-oriented substrates. We demonstrate that these characteristics can be explained from the view point of the lattice mismatch. Having established the decisive role of the strain, we present a mechanism that accounts for the symmetry-mismatched *M*-plane growth on (111)-oriented substrates by SSE.

II. EXPERIMENT

The MnAs growth was carried out using solid-source MBE for substrate orientations listed in Table I. In each case, following the growth of a GaAs buffer layer at 600 °C, a nominally 2-nm-thick MnAs layer was deposited at 200 °C with a growth rate of 0.3 nm/min and an As_4/Mn beam-equivalent pressure (BEP) ratio of 380. (The deposi-

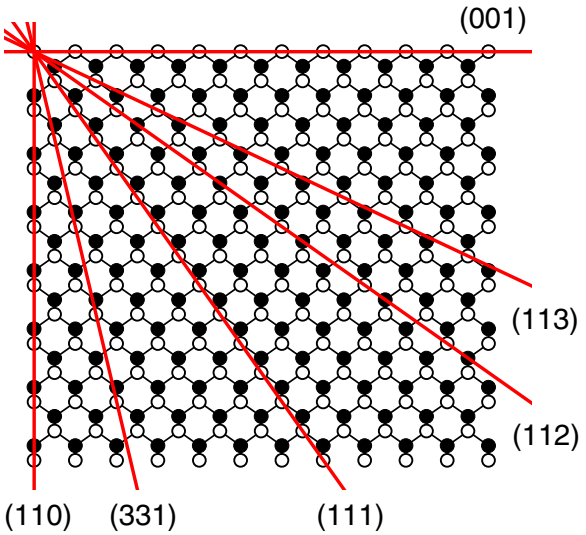

FIG. 1. (Color online) Crystal planes used in this study. GaAs is viewed in the $[\bar{1}10]$ direction.

TABLE I. Orientations of the GaAs substrates and the MnAs layers grown by solid-state epitaxy. The layer thickness and the deposition temperature of the amorphous MnAs are also listed. The alignment indicates the directions of the GaAs substrates to which the [0001] and $[11\bar{2}0]$ directions of the $(1\bar{1}00)$-oriented MnAs layers are parallel. Sample 1a contains components having the *c* axis rotated in plane by 60°, see Ref. 2. The fractions were estimated taking into account the structure and Lorentz-polarization factors of the reflections.

Sample	GaAs	MnAs	Thickness (nm)	Temperature (°C)	Alignment [0001], $[11\bar{2}0]$
#1a	(001)	$(1\bar{1}01)$ (70%)	20	180	
		$(1\bar{1}00)$ (30%)			[110], $[\bar{1}10]$ (~33%)
					60°-rotations (~67%)
#1b	(001)	$(1\bar{1}00)$ (66%)	130	200	[110], $[\bar{1}10]$ (70%)
					$[\bar{1}10]$, [110] (30%)
		$(1\bar{1}01)$ (17%)			
		$(2\bar{3}11)$ (12%)			
		$(11\bar{2}0)$ (~1%)			
		$(2\bar{2}01)$ (~1%)			
		$(1\bar{1}02)$ (~1%)			
#2a	(113)A	—	20	180	
#2b	(113)A	$(2\bar{3}11)$ (~100%)	150	200	
		(0001) (<1%)			
#3	(112)B	$(1\bar{1}01)$	135	200	
		$(2\bar{2}01)$			
		$(3\bar{3}02)$			
#4	(111)B	$(1\bar{1}00)$ (88%)	50	200	$\{11\bar{2}\}$, $\{\bar{1}10\}$
		$(1\bar{1}01)$ (12%)			
#5	(331)B	12°-tilted $(1\bar{1}00)$	125	200	
		5°-tilted $(11\bar{2}2)$			
#6	(110)	$(1\bar{1}00)$	135	200	[001], $[\bar{1}10]$

tion temperature was 180 °C for samples 1a and 2a. The BEP ratio was 420 for samples 1a, 2a, and 4.) During the deposition of MnAs, the reflection-high-energy-electron-diffraction (RHEED) pattern originating from the GaAs buffer layer vanished,[10] indicating the amorphous nature of the MnAs layer. Solid-state crystallization was then induced by enhancing the surface migration, i.e., closing the shutter for the As cell and increasing the substrate temperature to 250 °C. A RHEED pattern with distinct reflections emerged at the end of this procedure. Further growth of MnAs was then performed at 250 °C by means of conventional MBE with a growth rate of 3 nm/min and a BEP ratio of 28. Apart from an occasional change in the intensity, the RHEED pattern essentially remained unchanged during this conventional growth.

In Fig. 2, we compare the surface morphology of the MnAs layers obtained using scanning-electron micrography. The layers roughen as the substrate orientation is tilted from (110) toward (001). In the following, we will show that this roughening is a consequence of the lattice mismatch which increases from virtually zero for (110) to a very large value for (001) (note that this dependence is not, in general, a monotonic one[11]).

The epitaxial orientation relationship was determined using x-ray diffraction (XRD) ω-2θ scans over a wide angular range, as shown in Fig. 3 and summarized in Table I. These scans reveal that the MnAs layers grown on (110)- and (111)-oriented substrates are predominantly $(1\bar{1}00)$ oriented. The *c* axis of MnAs is aligned in a unique in-plane direction for GaAs(110). The monocrystalline nature of the layer is evidenced also by the well-developed quasiregular stripes of alternating α- and β-MnAs in Fig. 2(g).[12] For GaAs(111)B, the hexagonal prism of MnAs is aligned along one of six equivalent directions.[2] This multiplicity is inevitable due to the threefold symmetry of the GaAs(111) surface. In Fig. 2(e), elongated domains having sizes of several hundred nanometers are seen to be aligned along the GaAs$\{\bar{1}10\}$ direction. The *c* axis of MnAs is orthogonal to the elongation as MnAs[0001]$\|$GaAs$\{11\bar{2}\}$. The magnetic easy axis is hence parallel to the direction of the elongation.

The α-β stripes are apparent also for the MnAs layer on GaAs(331)B, Fig. 2(f). According to XRD (not shown),

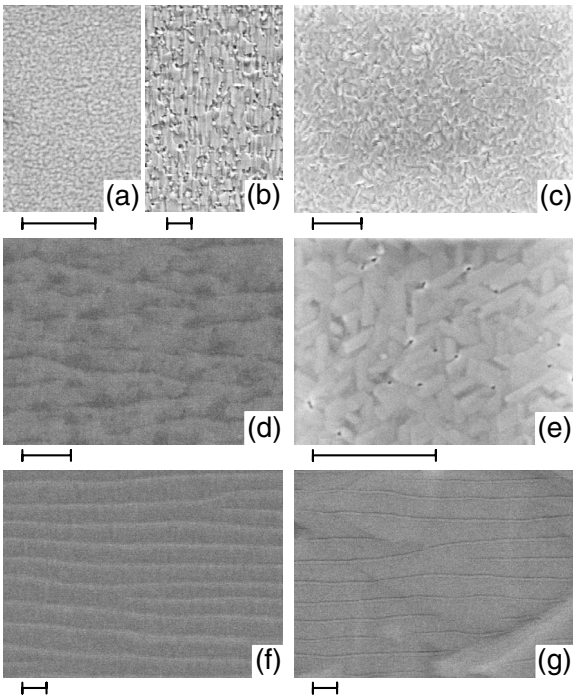

FIG. 2. Scanning-electron micrographs of samples (a) 1a, (b) 1b, (c) 2b, (d) 3, (e) 4, (f) 5, and (g) 6. The $[\bar{1}10]$ direction of the GaAs substrates is set to be in the vertical direction. The scale bars are 1 μm long

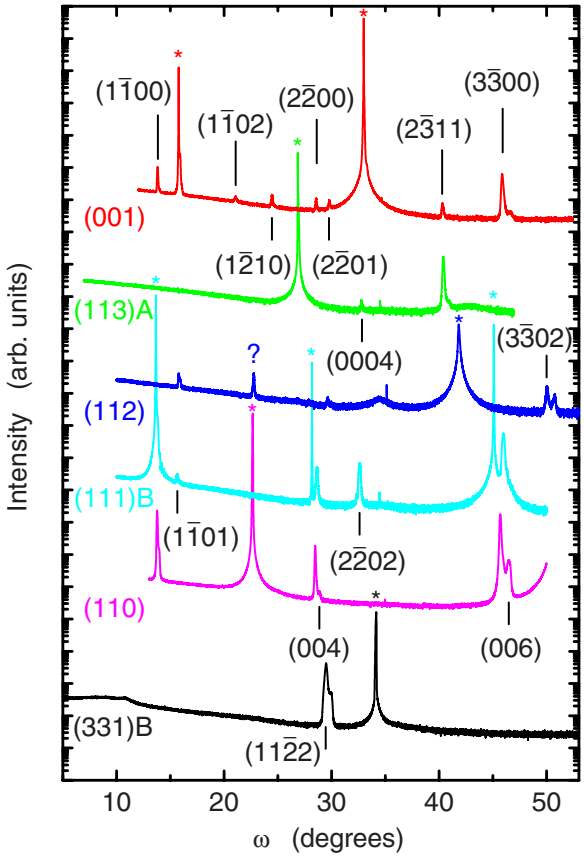

FIG. 3. (Color online) X-ray diffraction ω-2θ scans obtained from samples 1b, 2b, 3, 4, 6, and 5 for the curves from top to bottom, respectively. Reflections denoted with three indices stem from β-MnAs. Stars indicate reflections associated with the GaAs substrates. For sample 4, the peaks associated with the $(1\bar{1}00)$-oriented MnAs and those due to the substrate nearly overlap with each other. Peaks due to the MnAs layer emerged only when the specimen was tilted for sample 5. The tilt is 5° around the $[\bar{1}10]$ direction of the substrate for the bottom curve. The curves are offset for clarity.

however, the stripes appear to originate from the $(1\bar{1}00)$-oriented MnAs layer on a GaAs(110) terrace presumably exposed by step bunching.[13] An inclined $(11\bar{2}2)$ orientation of MnAs was additionally detected by XRD with a comparable peak amplitude. The bottom curve in Fig. 3 was obtained by tilting the specimen by 5° around the $[\bar{1}10]$ direction of the substrate. As the sample was rotated in the direction opposite to the rotation for detecting the peaks associated with the MnAs$(1\bar{1}00)$ layer, the MnAs$(11\bar{2}2)$ layer is assumed to have grown on the side surface of the terraces comprised of bunched steps.

When the substrate is GaAs(112)B, relatively coarse α-β stripes are again present in Fig. 2(d). Here, XRD indicates that the layer is a mixture of $(1\bar{1}0l)$ orientations. Notice that all the stripes in Figs. 2(d), 2(f), and 2(g) stretch in the same manner, indicating that the MnAs$[11\bar{2}0]$ direction is aligned, at least predominantly, along the common GaAs$[\bar{1}10]$ direction.

In contrast, the MnAs layers on GaAs(001) and GaAs(113)A consist of sub-micrometer-size grains, Figs. 2(a)–2(c). A number of surface orientations were identified by XRD as well as RHEED. We emphasize that no peak associated with the MnAs layer was found by XRD for sample 2a, suggesting that the layer mostly consists of microcrystallites that remain undetected by XRD due to a large peak broadening. While two surface orientations emerged for sample 2b, it is likely that the majority of MnAs in the layer is again present as microcrystallites of, therefore, unknown orientations. We note that the MnAs layer was deposited at 180 °C instead of 200 °C for sample 2a. The appearance of MnAs peaks in the XRD curve of sample 2b may be ascribed to the higher substrate temperature, besides the one-order-of-magnitude increase of the signal intensity due to the thickness. The MnAs layers on GaAs(001) manifest a sensitivity to the deposition temperature in terms of the morphology, Figs. 2(a) and 2(b), and the orientation relationship, see Table I.

III. LATTICE MISMATCH

The dependence of the surface morphology on the substrate orientation can be explained by the lattice mismatch.[14] We consider a situation in which a MnAs$(1\bar{1}00)$ layer is placed on a GaAs substrate. As verified by XRD, the $[11\bar{2}0]$ direction of the $(1\bar{1}00)$-oriented MnAs layers is exclusively aligned along the $[\bar{1}10]$ direction of GaAs. The comparatively moderate 8% lattice mismatch in this direction is

TABLE II. Ratio of the unit-cell length u of various GaAs surfaces and the c-axis lattice constant c of MnAs.

Surface	(001)	(113)	(112)	(111)	(331)	(110)
u (Å)	4.00	6.64	9.80	3.47	8.72	5.66
u/c	0.69	1.15	1.69	0.60	1.51	0.98
$2u/c$				0.997(6/5)	3.01	

known to be accommodated via the formation of a semicoherent interface having a periodic array of localized misfit dislocations.[15] We can, therefore, ignore the influence of this common lattice mismatch, and restrict our attention to the mismatch in the direction of MnAs[0001].

The length u of a unit cell on the GaAs surface changes irregularly with the surface orientation, see Table II. We hence inspect the match of the participating lattices for each substrate orientation. For the GaAs(110) substrate, the c-axis lattice constant c of MnAs is almost identical to u, in accordance with the nearly ideal MnAs growth.[16] As the spin lifetime is long on GaAs(110) surfaces due to the weak spin-orbit scattering,[17] the MnAs/GaAs(110) heterostructure is intriguing for spintronics. In fact, ω scans of both symmetric and asymmetric reflections (not shown here) for the SSE-grown layer are 15% narrower than those for a corresponding layer grown by conventional MBE, i.e., SSE leads to a smaller orientational spread and thus a higher crystal quality compared to conventional MBE.

For the GaAs(331) substrate, the ratio u/c is close to the fraction 3/2. The hexagonal structure of MnAs consists of two alternating planes of Mn and As in the c-axis direction, and so the effective unit-cell length is $c/2$ so long as the matching of the lattices is concerned. This means that three Mn and As planes fit in a unit length of GaAs. Therefore, a nearly mismatch-free growth is expected for MnAs$(1\bar{1}00)$/GaAs(331). We emphasize that the smooth surface observed in Fig. 2(f) is almost certainly due to the exposure of the GaAs(110) surface by step bunching. As step-bunching is robust on the GaAs(331)B surface, an experimental confirmation of the nearly mismatch-free growth of MnAs may be difficult.

The mismatch is, on the contrary, large for the (001)-, (113)-, and (112)-oriented substrates. A number of surface orientations that include out-of-plane tilts are realized in the MnAs layers on these substrates. In conventional MBE, smooth $(1\bar{1}00)$-oriented MnAs layers grow on GaAs(001) and GaAs(113) under optimized growth conditions, unlike the grainy layers in Figs. 2(a)–2(c). The difference is attributed to the fact that the growth is dominated by the interfacial and bulk strain energies in conventional and SSE-based MBE, respectively. The orientation relationship in conventional MBE is established when the layer thickness is minimal. The layer can easily stretch and thus gives priority to avoiding broken bonds. In SSE-based growth, the interfacial energy is insignificant in comparison to the strain energy accumulated in the already sizable volume of the layer at the moment of setting the epitaxial orientation. That is, the strain energy dominates over the interfacial energy (and the self-energy of misfit dislocations) as the layer thickness has exceeded the critical value for coherent growth. As there exists no specific low-energy epitaxial orientation for these substrates, multiple orientations having roughly comparable strain energies are generated to coexist.

The c axis is exclusively or dominantly aligned along the GaAs[110] direction in the SSE-based growth on GaAs(001). This indicates that, if the strain energies are comparable, other energy terms can influence the epitaxial orientation relationship. The c axis of MnAs in conventional growth is aligned along the GaAs[110] direction for the Mn-rich condition, whereas the alignment is along the GaAs$[1\bar{1}0]$ direction for the As-rich condition.[18] The stoichiometry in the amorphous layer may have similarly affected the in-plane alignment.

IV. SYMMETRY-MISMATCHED GROWTH

We now examine the case of the MnAs layer on GaAs(111), in which the symmetry-mismatched growth takes place. The ratio u/c is about 0.60 for this substrate orientation. We interpret this as $u/(c/2) \approx 6/5$. A ratio given as $(n \pm 1)/n$, with n being an integer, is most efficient for the formation of a coincidence lattice:[19] every sixth MnAs(0002) plane fits every fifth GaAs$(11\bar{2})$ plane. The lattice coincidence enables a good epitaxial growth. However, the question remains why growth proceeds exhibiting the C plane in conventional MBE but the M plane in SSE. The answer is the overwhelming importance of the strain energy in SSE.

Figure 4 illustrates the fit of the atomic configurations of MnAs and GaAs. For the symmetry-matched case, Fig. 4(a), broken bonds can be eliminated significantly by incorporating misfit dislocations in the form of a hexagonal network indicated by the dotted lines. This is the driving force for the C-plane orientation in conventional MBE. The misfit dislocations in the symmetry-mismatched MnAs$(1\bar{1}00)$/GaAs(111) system are anticipated to run parallel to the $[11\bar{2}]$ and $[\bar{1}10]$ directions of GaAs, Fig. 4(b). We list below three mechanisms that, with these configurations of dislocation networks, reduce the energy for the M plane to be lower than that for the C plane if residual strain is the only consideration.

First, a coincidence lattice, which occurs in the MnAs[0001] direction in Fig. 4(b), is obviously energetically favorable than an ordinary array of misfit dislocations, to which the case in Fig. 4(a) belongs. For a perfect coincidence lattice, the residual strain is almost completely restricted in the vicinity of the heterointerface over a distance given by

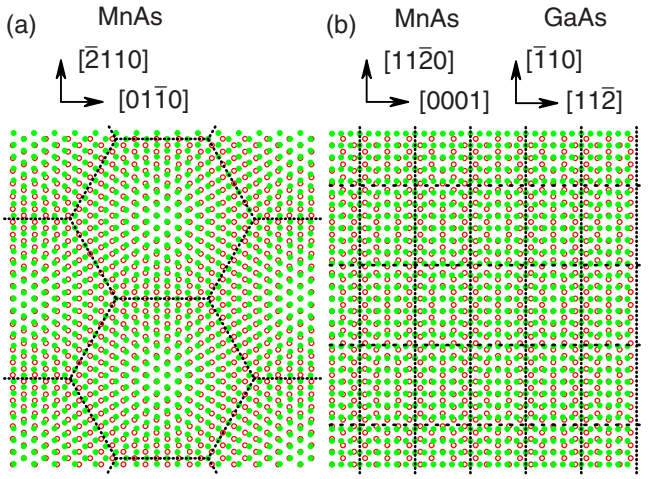

FIG. 4. (Color online) Schematic illustration of MnAs/GaAs(111) heterostructures for the (a) (0001) and (b) (1$\bar{1}$00) orientation of the MnAs layer. The lines indicate the network of misfit dislocations.

the period of the coincidence.[20] An approximate lattice coincidence occurs also for the MnAs[11$\bar{2}$0]‖GaAs[$\bar{1}$10] direction, as one finds in Fig. 4. The primary component of the residual strain is thus also localized at the interface. In the latter case, however, the deviation from perfect coincidence accumulates over periods of the approximate coincidence lattice to produce an eventual misfit. Such a slip in the periodic array of misfit dislocations is repeated hierarchically with algebraically increasing periods. These higher order arrays of "misfit dislocations" having extended strain distributions increase the strain energy when the ratio of the lattice constants is not a simple rational number, i.e., for the general case of noncoincidence lattice.

The other two mechanisms stem from the geometry of the dislocation networks and, therefore, make the *M*-plane orientation generally favorable regardless of the lattice constants. The periods of the dislocation array are roughly a half in Fig. 4(b) than in Fig. 4(a) even for the common MnAs[11$\bar{2}$0]‖GaAs[$\bar{1}$10] direction. The further relaxation of the residual strain reduces the strain energy for the *M*-plane case. Third, the strain field around the nodes in the dislocation network in Fig. 4(a) extends from the interface beyond the localization region imposed by the period. In Fig. 4(b), the two sets of misfit dislocations are orthogonal to each other, and so the strain relaxes in the two directions independently with efficient cancellation of the long-range strain field in each direction.[20] In contrast, at the nodes in Fig. 4(a), the dislocation needs to relax the strain two dimensionally.[21] The cancelation of the strain field around the nodes is doomed to be incomplete.

V. CONCLUSION

In conclusion, we have investigated the growth of MnAs layers on GaAs by means of SSE. The change in the crystallinity of the MnAs layers when the orientation of the GaAs substrates is varied faithfully reflects the residual strain in the layers. The dominance of the strain energy compared to the interfacial contribution of dangling bonds leads to the unusual realization of a symmetry-mismatched heterointerface in the case of GaAs(111). Due to the nature of the atomic bonding, the strain energy can readily overcome the interfacial energy for metal layers, and so SSE is more likely to produce unconventional orientation relationships in the growth of metal layers than semiconductor layers.

ACKNOWLEDGMENTS

The authors thank W. Braun for invaluable comments. Helpful conversations with A. Trampert, V. M. Kaganer, and R. Hey are also acknowledged.

[1] S. Stemmer, P. Pirouz, Y. Ikuhara, and R. F. Davis, Phys. Rev. Lett. **77**, 1797 (1996).
[2] Y. Takagaki, C. Herrmann, B. Jenichen, J. Herfort, and O. Brandt, Appl. Phys. Lett. **92**, 101918 (2008); **92**, 179901(E) (2008).
[3] L. Däweritz, Rep. Prog. Phys. **69**, 2581 (2006).
[4] M. Tanaka, Semicond. Sci. Technol. **17**, 327 (2002).
[5] M. Ramsteiner, H. Y. Hao, A. Kawaharazuka, H. J. Zhu, M. Kästner, R. Hey, L. Däweritz, H. T. Grahn, and K. H. Ploog, Phys. Rev. B **66**, 081304(R) (2002).
[6] J. Stephens, J. Berezovsky, J. P. McGuire, L. J. Sham, A. C. Gossard, and D. D. Awschalom, Phys. Rev. Lett. **93**, 097602 (2004).
[7] Y. Takagaki, E. Wiebicke, T. Hesjedal, H. Kostial, C. Herrmann, L. Däweritz, and K. H. Ploog, Appl. Phys. Lett. **83**, 2895 (2003).
[8] Y. Takagaki, L. Däweritz, and K. H. Ploog, Phys. Rev. B **75**, 035213 (2007).
[9] V. Garcia, Y. Sidis, M. Marangolo, F. Vidal, M. Eddrief, P. Bourges, F. Maccherozzi, F. Ott, G. Panaccione, and V. H. Etgens, Phys. Rev. Lett. **99**, 117205 (2007).
[10] A faint RHEED pattern already appeared at the end of the 2-nm-thick deposition for samples #2b and #6.
[11] W. Braun, V. M. Kaganer, A. Trampert, H.-P. Schönherr, Q. Gong, R. Nötzel, L. Däweritz, and K. H. Ploog, J. Cryst. Growth **227-228**, 51 (2001).
[12] V. M. Kaganer, B. Jenichen, F. Schippan, W. Braun, L. Däweritz, and K. H. Ploog, Phys. Rev. Lett. **85**, 341 (2000).
[13] R. Nötzel and K. H. Ploog, Jpn. J. Appl. Phys., Part 1 **39**, 4588 (2000).
[14] As the thermal expansion and the discontinuous lattice-constant change at the phase transition between the α and β phases of MnAs are large, we use the lattice constants at the growth temperature obtained from T. Suzuki and H. Ido, J. Phys. Soc. Jpn. **51**, 3149 (1982).
[15] A. Trampert, F. Schippan, L. Däweritz, and K. H. Ploog, Appl.

Phys. Lett. **78**, 2461 (2001).
[16] D. Kolovos-Vellianitis, C. Herrmann, L. Däweritz, and K. H. Ploog, Appl. Phys. Lett. **87**, 092505 (2005).
[17] Y. Ohno, R. Terauchi, T. Adachi, F. Matsukura, and H. Ohno, Phys. Rev. Lett. **83**, 4196 (1999).
[18] M. Tanaka, J. P. Harbison, M. C. Park, Y. S. Park, T. Shin, and G. M. Rothberg, Appl. Phys. Lett. **65**, 1964 (1994).
[19] A. Trampert and K. H. Ploog, Cryst. Res. Technol. **35**, 793 (2000).
[20] D. K. Satapathy, V. M. Kaganer, B. Jenichen, W. Braun, L. Däweritz, and K. H. Ploog, Phys. Rev. B **72**, 155303 (2005).
[21] T. D. Young, J. Kioseoglou, G. P. Dimitrakopulos, P. Dłużewski, and P. Komninou, J. Phys. D **40**, 4084 (2007).